Cu K -edge resonant inelastic x-ray scattering in edge-sharing cuprates

F. Vernay, B. Moritz, I. S Elfimov, J. Geck, D. Hawthorn, T. Devereaux, G. Sawatzky

Cu *K*-edge resonant inelastic x-ray scattering in edge-sharing cuprates

F. Vernay,[1,2] B. Moritz,[1,2,*] I. S. Elfimov,[3] J. Geck,[3] D. Hawthorn,[3] T. P. Devereaux,[1,2,*,†] and G. A. Sawatzky[2,3]
[1]*Department of Physics and Astronomy, University of Waterloo, Waterloo, Ontario N2L 3GI, Canada*
[2]*Pacific Institute of Theoretical Physics, University of British Columbia, Vancouver, V6T 1Z1 BC*
[3]*Department of Physics, University of British Columbia, Vancouver, V6T 1Z4 BC*
(Received 1 October 2007; published 18 March 2008)

We present calculations for resonant inelastic x-ray scattering (RIXS) in edge-shared copper oxide systems, such as Li_2CuO_2 and $CuGeO_3$, appropriate for hard x-ray scattering, such as the copper *K* edge. We perform exact diagonalizations of the multiband Hubbard model and determine the energies, orbital character, and resonance profiles of excitations which can be probed via RIXS. We find excellent agreement with recent results on Li_2CuO_2 and $CuGeO_3$ in the 2–7 eV photon energy loss range.

DOI: 10.1103/PhysRevB.77.104519 PACS number(s): 74.25.Jb, 74.72.−h, 78.20.Bh, 78.70.Ck

I. INTRODUCTION

Techniques that probe the momentum dependence of strongly correlated electrons provide valuable information that can be used as a test for models appropriate for the cuprates. Angle-resolved photoemission (ARPES) provides important information about single-particle excitations of occupied states.[1,2] Electronic Raman scattering reveals information about multiparticle excitations at long wavelengths.[3] Resonant inelastic x-ray scattering (RIXS), a form of Raman spectroscopy, recently has undergone vast improvements, allowing probes of momentum-dependent excitations into unoccupied states.[4] Improvements in resolution now offer the possibility of a direct comparison of ARPES, Raman, and RIXS spectra in the several eV range with the hope of understanding the nature of strong correlations in the cuprates, and high temperature superconductivity, by studying electronic excitations at several energy scales.

As a fundamental building block of low-energy effective theories of the cuprates, the Zhang-Rice singlet (ZRS)[5] is the starting point of the single-band Hubbard and t-J models widely believed to capture the low-energy physics of strongly correlated systems. It is well known that the ZRS features prominently in RIXS in the cuprates. A particular test of models of the cuprates lies in the difference between RIXS in edge-shared versus corner-shared copper oxide systems. In materials such as La_2CuO_4 and other corner sharing two-dimensional members of the high T_c family, the ZRS is stabilized by a strong gain in antiferromagnetic exchange energy between Cu and O, and can propagate to neighboring CuO_4 plaquettes, with effective hopping $t=-0.35$ eV along the Cu-O bond direction, and $t'=0.15$ eV along the diagonal.[5] In edge-shared cuprates, such as Li_2CuO_2 and $CuGeO_3$, the Cu-O-Cu bond approximately forms a 90° angle,[6] compared to 180° in corner-shared cuprates, and therefore according to Goodenough-Kanamori-Anderson,[7] the nearest-neighbor copper-copper exchange tends to be slightly ferromagnetic. However, higher order processes such as Cu-O-O-Cu hopping also contribute comparable antiferromagnetic exchange terms. For these reasons, small bond-angle variations among different edge-sharing compounds can make the exchange slightly antiferromagnetic or ferromagnetic. In either case, the ZRS is less stable and mobile due to the hybridization among different oxygen orbitals not aligned with Cu $d_{x^2-y^2}$ orbitals.[6]

Recent Cu *K*-edge RIXS data on edge-sharing cuprate Li_2CuO_2 (Refs. 8 and 9) has revealed a small, nondispersive peak at 2.1 eV, attributed to interatomic *d*-*d* excitations, a strong peak at 5.4 eV and a weak peak at 7.6 eV, both attributed to charge transfer excitations. The peak at 5.4 eV is doubly resonant for incident photon energies near 8986 and 9000 eV.[8] In $CuGeO_3$, clear excitations were found, 3.8 eV (weak) and 6 eV (strong),[9–11] and more recently 1.7 eV,[12] which were attributed in Ref. 12 as a intra-atomic *d*-*d* excitation (1.7 eV), a ZRS excitation (3.8 eV), and a charge transfer excitation on a single copper oxide plaquette (6.4 eV). Similar features have also appeared in oxygen 1*s* RIXS.[13] While a few momentum-dependent studies have been performed, the incident photon energy dependence, or resonance profile, is usually shown only for a few selected points in the Brillouin zone.

In this paper, we present a theory for RIXS for the copper *K*-edge and present exact diagonalizations of Hubbard clusters of edge-sharing copper oxide plaquettes shown in Fig. 1. We calculate both the RIXS spectrum and the resonance profile for several cluster geometries, and determine the nature of excitations accessible via light scattering. We pay specific attention to the intermediate core-hole and final excited-state wave functions of RIXS accessible states. We find good agreement with the results on edge-shared copper oxide systems, and confirm a number of previous excitation assignments.[10–12]

II. MODEL AND METHOD

A. Resonant inelastic x-ray scattering process

The RIXS process consists in scattering an incident photon of energy $\hbar\omega_I$ off a sample in the ground state $|\psi_0\rangle$ having energy E_0. For *K*-edge RIXS, an electron from the 1*s* copper core is photoexcited into the Cu 4*p* band, leaving behind a core hole. The strong Coulomb repulsion between the core hole and $d_{x^2-y^2}$ holes on the same Cu atom reorganizes charge density, forming an intermediate state $|\psi_{ci}\rangle$ of eigenenergy E_{ci}. The 4*p* electron resides in a rather extended wave function and therefore interacts weakly with *d* and core

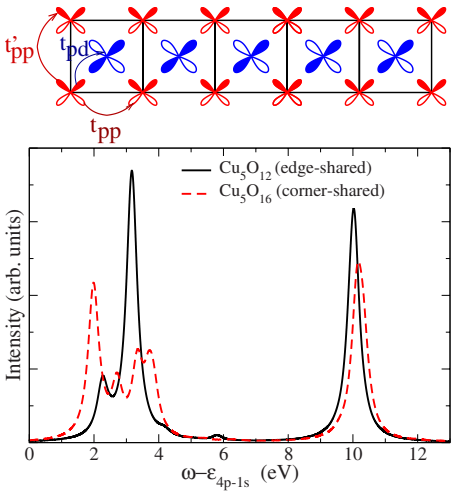

FIG. 1. (Color online) Top: Edge-shared Cu_5O_{12} cluster. Bottom: XPS spectrum as a function of photon energy transfer and incident photon energy, for corner and edge-sharing copper-oxide clusters.

states. We neglect its interaction hence providing us with a rather simple description of RIXS. The $4p$ electrons then enter into the problem as a spectator at energy $\epsilon_{4p}=\hbar\omega_I-(E_{ci}-E_0)$ and the intensity will be proportional to the projected $4p$-band density of states (DOS) at that energy. The incident polarization determines the necessary orbital projection. The $4p$ electron then recombines with the $1s$ core-hole emitting a photon of energy $\hbar\omega_F$, leaving the system in the final state $|\psi_f\rangle$ of eigenenergy E_F and a photon energy transfer $\hbar\Omega=\hbar\omega_I-\hbar\omega_F$. This leads to a simplification of the general expression given in Ref. 4. In this approximation, the spectrum will be given by the following relation and with the $\hbar\omega_I$ dependence given by a convolution with the $4p$ band DOS:

$$I(\omega_I,\Omega=\omega_I-\omega_F) \propto \sum_f \left| \sum_i \sum_{4p} \frac{\langle\psi_f|\psi_{ci}\rangle\langle\psi_{ci}|\psi_0\rangle}{E_{ci}+\epsilon_{4p-1s}-E_0-\hbar\omega_I-i\Gamma_1} \right|^2 \times \delta(E_F-E_I-\hbar\Omega). \quad (1)$$

Here $\epsilon_{4p\text{-}1s}$ represents the Cu $1s$-$4p$ energy separation. For simplicity, in a first approach, we neglect specific $4p$ orientation and photon polarizations. The polarization dependence, as well as the related $4p$ orientation and the $4p$ projected DOS, will be discussed in the last part of Sec. III. The parameter Γ_1 represents damping of the intermediate state due to the fluorescence and Auger $1s$ decay, which we take as 1.0 eV. While this value determines the overall resonant enhancement, it does not affect the resolution of the energy-loss peaks in the spectrum. We broaden the delta function with a width 0.1 eV to represent current instrument resolution. We note that in Eq. (1), the states $|\psi_{ci}\rangle$ are identical to those in a core x-ray photoemission experiment.

The Hamiltonian describing the open boundary cluster shown in Fig. 1, with rotated x and y local directions along the p orbitals, is given by $\mathcal{H}=\Sigma_{\langle i,j\rangle,\sigma}\mathcal{H}^K_{ij\sigma}+\Sigma_i(\Sigma_\sigma\mathcal{H}^\epsilon_i+\mathcal{H}^U_i)+U_Q\Sigma_{\sigma,\sigma'}d^\dagger_{0,\sigma}d_{0,\sigma}[1-s^\dagger_{0,\sigma'}s_{0,\sigma'}]$, with $H_i\epsilon$ containing the site energies and

$$\mathcal{H}^K_{ij\sigma}=t_{pd}P_{i,j}p^\dagger_{i,\sigma}d_{j,\sigma}+t_{pd_z}P^z_{i,j}p^\dagger_{i,\sigma}d_{z,j,\sigma}+t_{pp}P'_{i,j}p^\dagger_{i,\sigma}p_{j,\sigma}+t'_{pp}p^{\dagger\prime}_{i,\sigma}p_{j,\sigma}+\text{H.c.}$$

$$\mathcal{H}^U_i=U_{pp}p^\dagger_{i,\uparrow}p_{i,\uparrow}p^\dagger_{i,\downarrow}p_{i,\downarrow}+U_{pp}p^{\dagger\prime}_{i,\uparrow}p'_{i,\uparrow}p^{\dagger\prime}_{i,\downarrow}p'_{i,\downarrow}+U_{dd}d^\dagger_{i,\uparrow}d_{i,\uparrow}d^\dagger_{i,\downarrow}d_{i,\downarrow}+U_{dd}d^\dagger_{z_{i,\uparrow}}d_{z_{i,\uparrow}}d^\dagger_{z_{i,\downarrow}}d_{z_{i,\downarrow}}.$$

Here, $d^\dagger_{i,\sigma},d^\dagger_{z_{i,\sigma}},p^\dagger_{i,\sigma},p^{\dagger\prime}_{i,\sigma}$ and $d_{i,\sigma},d_{z_{i,\sigma}},p_{i,\sigma},p'_{i,\sigma}$ create and annihilate a $d_{x^2-y^2}$, $d_{3z^2-r^2}$, planar p or p' hole with spin σ at site i, respectively, and the sum runs over nearest neighbors. The hopping amplitude t_{pp} refers to the hopping between two nearest p_x p_y orbitals, and t'_{pp} refers to the hopping between two nearest-neighbor p_α oxygen orbitals, where $\alpha=x,y$. The overlap phase factors are chosen such that $P_{i,j}=1$ for neighbors in the x, $-y$ direction, and -1 for $-x,y$. The oxygen phase factors are analogously defined as $P'_{i,j}=1$ for oxygen at x,y and $-x,-y$, and -1 for the other combinations. Here, $s^\dagger_0$ (respectively, s_0) creates (annihilates) a Cu_{1s} core electron, and U_Q is the core-d hole repulsion. For simplicity, we neglect interactions involving the $4p$ photoexcited electron, such as the $4p$-$3d$ Coulomb interactions. These include off-diagonal couplings between d states which may be important for singlet-triplet energy differences as well as providing pathways for symmetry-allowed d-d excitations. We also neglect exchange interactions involving the $1s$ core hole, which are very small.

In what follows, we use a standard set of parameters (in eV):[5] $t_{pd}=1.1$, $t_{pp}=0.5$, $t'_{pp}=-0.538\times t_{pp}$, $\epsilon_d=0$, $\epsilon_{dz}=1.7$, $\Delta=\epsilon_p-\epsilon_d=3.5$, $U_{pp}=6$, $U_{dd}=8.8$, and $U_Q=8$. These parameters give a value for the copper magnetic exchange $J=0.14$ eV for corner-shared copper oxides, and 2.8 meV for edge shared.

B. Discussion of the method and comparison with previous works

We first perform full exact diagonalization of the Hamiltonian without the core hole, and then redo the calculation with the core hole. Since the Hamiltonian conserves the total spin, we diagonalized in the $S=1/2$ sector. From the eigenvalues and eigenvectors of the two steps, the RIXS spectrum for a given $\hbar\omega_I$ is computed from Eq. (1).

As our calculations involve determining the eigenvector of each state used to construct the matrix elements involved in RIXS, we know the character of each excitation exactly and do not need to make *a priori* assumptions about which peak corresponds to which fundamental excitation. This allows us to make direct correspondence between RIXS and other core-level spectroscopic techniques, without any further assumptions.

This is quite different from the Lanczos method, which truncates the Hilbert space and focuses on the low-lying energy excitations. Whereas this method allows investigation of slightly larger clusters, extensions to higher energies is problematic particularly for RIXS where eigenvectors are needed to evaluate the matrix elements between higher en-

ergy states in order to obtain both the resonance profile (dependence on incident photon energies) as well as the intensities of prominent peaks in the spectrum. Since the core-hole interaction is essentially local in nature (on-site Coulomb repulsion), leading to only a slight delocalization of the charge, we checked that the cluster size does not play a crucial role in the qualitative shape of the spectra. In that sense, the calculations done in the present paper add more information and provide a more direct access to the relevant RIXS excitations compared to other techniques used in previous studies in the context of standard cuprates.[14] These studies treated the one-band Hubbard model where the Zhang-Rice singlets are, by construction, already formed, and focused only on the momentum dependence of the Mott gap excitation. By treating the problem in a multiband model, the formation of Zhang-Rice excitations comes naturally in the problem and its signature in the RIXS intensity, peak dispersion, and resonance profile can be directly addressed. In fact, it is widely recognized that the gap is a charge transfer gap which involves transition from oxygen $2p$ to copper $3d$ states.[15]

III. RESULTS AND DISCUSSIONS

A. Preliminary remarks

In core level x-ray photoelectron spectroscopy (XPS), the final state corresponds to an intermediate state in the RIXS process. We first plot the XPS spectrum for both edge-shared cluster Cu_5O_{12} and corner-shared cluster Cu_5O_{16} in Fig. 1. In both cases, the prominent features correspond largely to (1) a nonlocally screened d-intersite ZRS (d^9L) feature at 2.2 eV, where the core hole has pushed a d^9 hole from the on-site Cu onto the oxygen ligands in the neighboring plaquette; (2) a local charge transfer (CT) excitation ($d^{10}L$) at 3.5 eV, whereby the screening of the core hole comes from the hole transfer from copper to oxygen on the same plaquette;[16] and (3) a 10 eV high-energy poorly screened d^9 Cu hole on the core-hole site. These results are quantitatively similar to those presented earlier,[17] apart from a more realistic value of the exchange J in the corner-shared geometry. We note that x-ray absorption spectra in an extended system can be obtained from our XPS spectrum via a convolution with the copper $4p$ DOS, giving a broad absorption edge followed by spectral intensity extending higher in energy governed by the $4p$ bandwidth.

These excitations, present in both corner- and edge-shared geometries, occur at roughly the same energy since they are governed by charge transfer energies and the exchange $\propto t_{pd}^2/\Delta$ between copper and oxygen: the Cu-Cu exchange does not play a major role in setting these energy scales.

The main difference concerns the prominence of the nonlocally screened d-intersite ZRS excitation in the corner-shared compared with the edge-shared systems. While the ZRS accounts for nearly 80% of the ground state wave function including the core hole for the corner-shared plaquettes, it is approximately 56% for the edge-shared system, reflecting the number of oxygen hybridization pathways available in the edge-shared configuration.[18] Thus, while the energy is comparable in both systems, the matrix elements are much

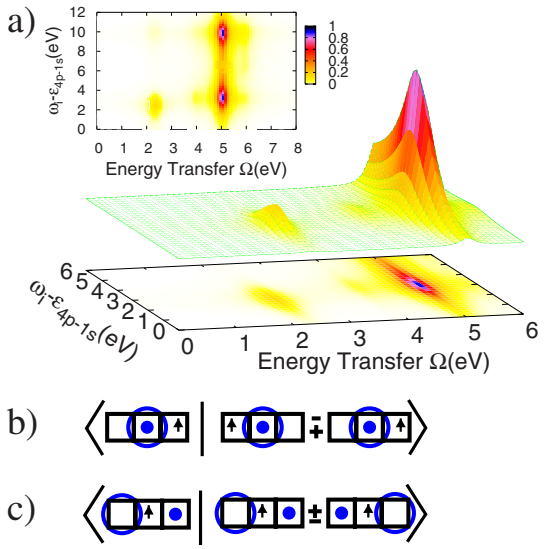

FIG. 2. (Color online) (a) RIXS spectra for Cu_3O_8 cluster as a function of photon energy transfer Ω and incident photon energy ω_I, measured relative to the binding energy ϵ_{4p-1s}. The inset shows a contour map over large frequencies. Matrix elements for Cu_3O_8 are shown in (b) and (c), for the main peaks in RIXS at $(\omega_i - \epsilon_{4p-1s}, \Omega) = (2.2, 2.2)$ and (3.1,5.07), eV respectively. Here, the left and right eigenvectors is the core hole and final states, respectively, and the dot and the circle represent a singlet state formed by a hole on the copper site (dot) and a hole delocalized on the oxygens having the ZR symmetry (circle).

weaker at the ZRS scale in the edge-shared compared to corner-shared systems. In addition, the mobility of the ZRS for each geometry determines the peak widths, reflecting the splitting between bonding and antibonding ZRSs on sites neighboring the core hole. In the case of the corner-shared systems, this corresponds to $2t = -0.7$ eV, while due to the orientation of the orbitals in the edge-shared systems, the splitting is $2t' = 0.3$ eV. As a result, the locally screened $d^{10}L$ peak at 3.1 eV is much larger in edge shared compared to corner shared. This has led the phenomenon of high-temperature superconductivity, occurring in corner-shared compounds and absent in edge-shared compounds, to be associated with the stability of the ZRS.[19] We note that the primary role of the oxygen orientation in the formation of the ZRS is not captured in single-band Hubbard model calculations.

B. Resonant inelastic x-ray scattering results: Attribution of the peaks

The aim of this section is to discuss the overall shape of the RIXS spectrum and resonant profile for a Cu_3O_8 cluster in the inset of Fig. 2(a). We show how to attribute to each peak the corresponding excitation, as an example, we have chosen the same parameters as for XPS in Fig. 1, appropriate for Li_2CuO_2. From here on, we set $\hbar$ equal to 1. Here, the intermediate state core hole is included on the edge of the cluster. The calculations are also performed for different locations of the core hole on the cluster, which has one hole per copper plaquette. While the results differ slightly for dif-

ferent locations of the core hole, we note that the changes are only quantitative and give different broadening of the RIXS peaks due to the different mobilities, of the *d*-intersite Zhang-Rice excitation on the end or middle of the cluster. However, since the aim of this paper is to compare trends for different cluster geometries and charge transfer energies, we will not discuss further these relatively minor changes in the spectra.

The RIXS spectrum shown in the inset of Fig. 2(a) consists of two prominent excitations at approximately $\Omega = 5.07$ eV energy transfer, at incident photon energies of 3.1 and 10 eV. This is the local CT excitation, resonant at both the locally screened $d^{10}L$ CT and poorly screened d^9 intermediate states, as shown in Fig. 1. In addition, a weaker *d*-intersite ZRS-derived peak is present at $\Omega = 2.2$ eV, resonant for incident photon energies near 2.2 eV above the $1s$-$4p$ transition. The XPS spectra may be crudely viewed as a sum over all Raman shifts of the RIXS spectrum as a function of the incident photon energy $\hbar\omega_I$.

In Fig. 2(a), we show a blow up of the low-energy RIXS spectrum. By examining the symmetries of the core hole and final state wave functions, the nature of the RIXS excitations, and the origin of their resonant profile, can be determined by inspection of matrix elements appearing in Eq. (1). The ground state without the core hole $|\psi_0\rangle$ is largely of d^9 character in each plaquette. Only those intermediate states which have a large overlap with the ground state are relevant to the RIXS process. To determine which final states $|\psi_{i\neq 0}\rangle$ are probed by RIXS and at what resonant energy they occur, one inspects the overlap of the core-hole states $|\psi_c\rangle$ reachable via the ground state without the core hole $|\psi_0\rangle$, with other excited states $|\psi_{i\neq 0}\rangle$ in the same Hilbert space. For example, since the ground state of the cluster $|\psi_0\rangle$ is a singlet, it cannot be coupled to triplet intermediate states having a core hole. We immediately conclude that for our cluster, all triplet states do not appear in the RIXS process without spin-orbit coupling.

We sketch schematically in Figs. 2(b) and 2(c) the leading order contributions to the wave functions of the intermediate state with the core hole and the final state with large matrix overlap, which correspond to the main excitations shown in the RIXS spectra. While the intermediate state is predominantly one configuration, the final states can either be bonding or antibonding combinations of excitations on the plaquettes, at energies approximately 2 eV above E_0, split by ZRS hopping.

In Fig. 2(b), it is clear that the resonance peak at $\omega - \epsilon_{4p\text{-}1s} = 2.2$ eV and energy transfer $\Omega = 2.2$ eV come from the combination of intermediate and final states corresponding to the creation of the ZRS in the final state, having strong overlap with the nonlocal, well-screened d^9L intermediate state. The two final states of bonding and antibonding combinations of ZRS on the two plaquettes couple to the intermediate state, with a weak splitting in edge-shared systems. Even with our broadening of 0.1 eV, the separate peaks are difficult to resolve.

The final states of the higher energy peak correspond to bonding and antibonding combinations of $d^{10}L$, having strong overlap with the intermediate core-hole state with the ligand on the core-hole site, as shown in Fig. 2(c). This lies at higher energy $\omega_i - \epsilon_{4p\text{-}1s} = 3.07$ eV, and is the most prominent final state in XPS shown in Fig. 1.

We note that we do not find any prominent *d*-*d* excitations lying in the relevant energy range below 2 eV, even when including other *d* orbitals.[20] This follows from a symmetry analysis of the states, whereby d^9L and $d^{10}L$ configurations cannot hybridize other Cu *d* orbitals and combinations of oxygen ligands. Thus, direct *d*-*d* excitations are inaccessible in our model, in agreement with electron energy loss cluster calculations.[21] It is plausible that *d*-*d* excitations may arise if symmetry-breaking interactions with the $4p$ are included. This is different for oxygen $1s$ RIXS, as the creation of the core hole breaks this symmetry, allowing direct *d*-*d* excitations, as determined in recent cluster calculations.[22] Moreover, *d*-*d* excitations may arise from multiple couplings in nonresonant scattering[23] which are not treated in our calculation.

C. Influence of the 4*p* states: Polarization dependence–Material dependence

So far, our analysis did not include the copper-$4p$ states. However, in order to obtain results more closely connected to experiment and to include a photon polarization dependence for the Cu *K*-edge process, the Cu $4p$ DOS must be included into the calculations. Indeed, the Cu $1s$ core electron can only be excited into the $4p$ levels if there is a finite DOS for unoccupied states. Due to the crystal field effects, the $4p$ DOS for different $4p_{x,y,z}$ orbitals provides a polarization dependent shift of the resonance energies and secondary satellites governed by the peaks of each $4p$ projected DOS as well as the overall bandwidth. The orientation of the incident and emitted photon polarizations determine which $4p$ projected DOS is accessed.

Since the $4p$ states are rather extended orbitals, their interaction with the Hubbard subbands is quite weak. However, depending on the incoming light polarization, matrix elements are selected so that one can access different linear combinations of $4p_x$, $4p_y$, and $4p_z$ states. Since the DOS distributions are different, the RIXS spectra reflect these characteristics. Thus, to deduce the influence of the $4p$ states, we neglect minor real-space variations of the combined cluster-$4p$ wave function and compute the convolution of our raw-RIXS spectrum with the calculated $4p$ projected DOS $N_{4p}(\epsilon_{4p})$:

$$
\begin{aligned}
I(\omega_I, \Omega = \omega_I - \omega_F) \propto \sum_f \Bigg| \sum_i \int d\epsilon_{4p} N_{4p}(\epsilon_{4p}) \\
\times \frac{\langle \psi_f | \psi_{ci} \rangle \langle \psi_{ci} | \psi_0 \rangle}{E_{ci} + \epsilon_{4p-1s} - E_0 - \hbar\omega_I - i\Gamma_1} \Bigg|^2 \\
\times \delta(E_F - E_I - \hbar\Omega) \\
= \sum_f \left| \int d\epsilon_{4p} N_{4p}(\epsilon_{4p}) M(\hbar\omega_I - \epsilon_{4p-1s}, f) \right|^2 \\
\times \delta(E_F - E_I - \hbar\Omega),
\end{aligned}
$$

where

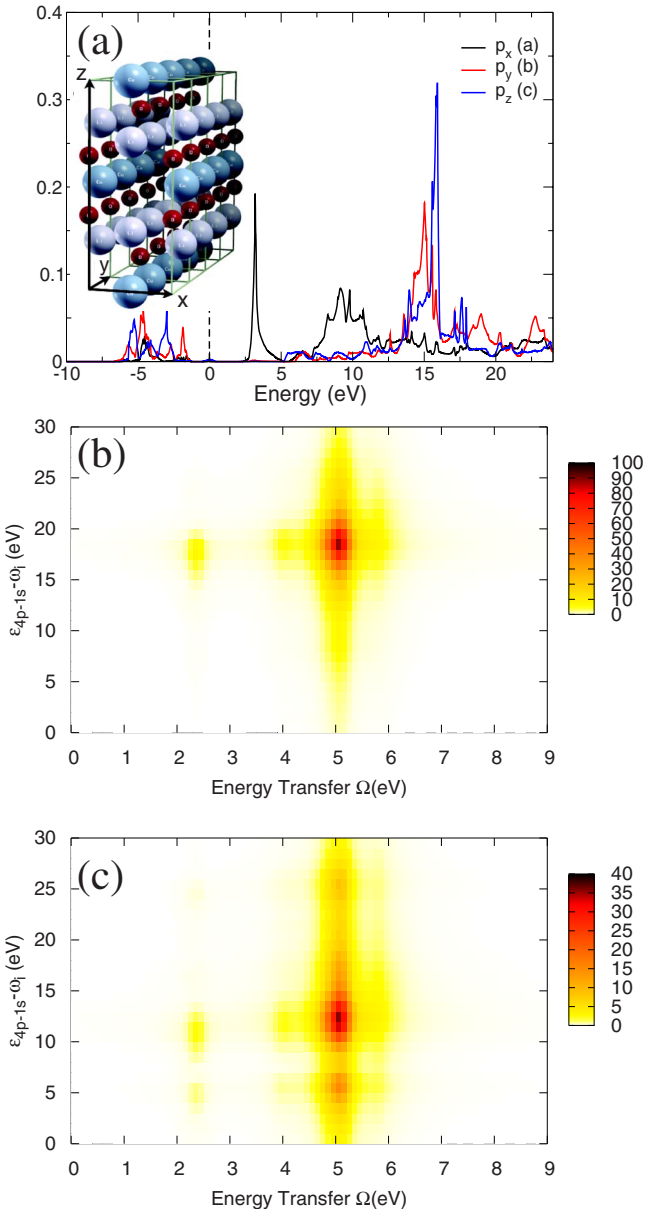

FIG. 3. (Color online) (a) Cu $4p$ partial density of states for Li_2CuO_2. (b) RIXS spectrum for parameters corresponding to Li_2CuO_2, convoluted with the p_z-DOS. (c) RIXS spectrum for parameters corresponding to Li_2CuO_2, convoluted with the p_x-DOS. For both (b) and (c), we took a core-hole lifetime of $\Gamma=1.5$ eV.

$$M(\hbar\omega_I,f)=\sum_i \frac{\langle\psi_f|\psi_{ci}\rangle\langle\psi_{ci}|\psi_0\rangle}{E_{ci}-E_0-\hbar\omega_I-i\Gamma_1}. \quad (2)$$

The projected $4p$ DOS is calculated using linearized augmented plane wave method (LAPW) in a coordinate system consistent with experiment.[24] In the following section, we present results for different edge-shared cuprates Li_2CuO_2 and $CuGeO_3$.

1. Li_2CuO_2

For Li_2CuO_2, the $4p$ projected DOS is shown in Fig. 3(a). The $4p_z$ DOS has two sharp peaks at roughly 17 eV, with subdominant peaks as shoulders to the main peak. The resulting RIXS spectrum for z photon polarizations shown in Fig. 3(b) thus has a shifted d-intersite ZRS resonance at $\epsilon_{4p}-\omega_i\sim 19$ eV instead of 2.2 eV in Fig. 2, yet remains sharply peaked even though the $4p_z$ bandwidth is over 20 eV wide. The $d^{10}L$ CT and poorly screened excitation at $\Omega\sim 5$ eV are likewise shifted to higher resonance frequencies.

The $4p_x$ DOS in Fig. 3(a) has a double-peak structure, with a single sharp peak at 4 eV and a tightly structured set of peaks around 10 eV. The resulting RIXS spectrum for photon polarizations along the x axis, given in Fig. 3(c), clearly shows two split resonances at $\sim$6–7 eV and $\sim$13 eV, a shift of the raw RIXS spectrum (Fig. 2) by the 4 eV and 10 eV $4p_x$ DOS peaks. The difference in the relative intensities between Figs. 3(b) and 3(c) is due to the fact that the DOS for the p_z orbitals is more intense at its maximum than for the p_x orbital.

Figure 4 displays a side-by-side comparison of the present theory and recent experimental data by Kim *et al.*[8] on Li_2CuO_2. The theory and experimental curves show striking similarities in both the energy transfer and the incoming photon energy range. The energy scale, prominence of the local CT excitation, and the double resonance profile shown in Figs. 1, 2, and 4 correspond well to the RIXS experiments. We remark that while Ref. 8 attributed the weak 2.1 eV peak to an interatomic d-d excitation, and the strong peak at 5.4 eV peak to local CT excitation, in view of our results, we may associate the low-energy excitation with the d-intersite ZRS excitation. We note that since we have not fine tuned the oxygen orbital orientations in Li_2CuO_2, the strength of this excitation may be overestimated. The weak peak observed at 7.6 eV, however, has no correspondence in our calculations. This peak may be associated with a local CT excitation into states with different ligand symmetries orthogonal to the ZRS ligand states, which may become accessible once oxygen $4p$-$2p$ interactions are included.

2. $CuGeO_3$

As pointed out in Ref. 6, the large valency of Ge^{4+} nearby the CuO planes increases the Madelung energy difference between the Cu and planar O sites in $CuGeO_3$ compared to $LiCuO_2$, leading to the values $\Delta=4.9$ and 3.2 eV, respectively, for each system. Since this energy scale largely determines the energies of the d-intersite ZRS and the separation in energy to the local CT excitation, the RIXS spectrum and resonance profile should be largely different in the two cases.

In a first approach, as we did for Li_2CuO_2, we present in Fig. 5 a nonconvoluted RIXS spectrum for parameters corresponding to $CuGeO_3$, which are the same set of parameters as before apart from the change $t_{pd}=1.23$ eV and $\Delta=4.9$ eV. The larger value of Δ leads to several changes compared to the RIXS spectrum for Li_2CuO_2 parameters [see Fig. 2(a)]. First, we note that the d-intersite ZRS peak has moved higher in energy from the d^9 and core-hole ground states, lying at a photon energy transfer Ω of 3.1 eV, and resonant at a higher incident photon energy $\omega_i-\epsilon_{4p\text{-}1s}=3.1$ eV. The bonding- antibonding splitting is smaller and the resonant peaks are more sharp. In addition, the CT ($d^{10}L$) excitations move higher in energy, lying at $\omega_i-\epsilon_{4p\text{-}1s}$

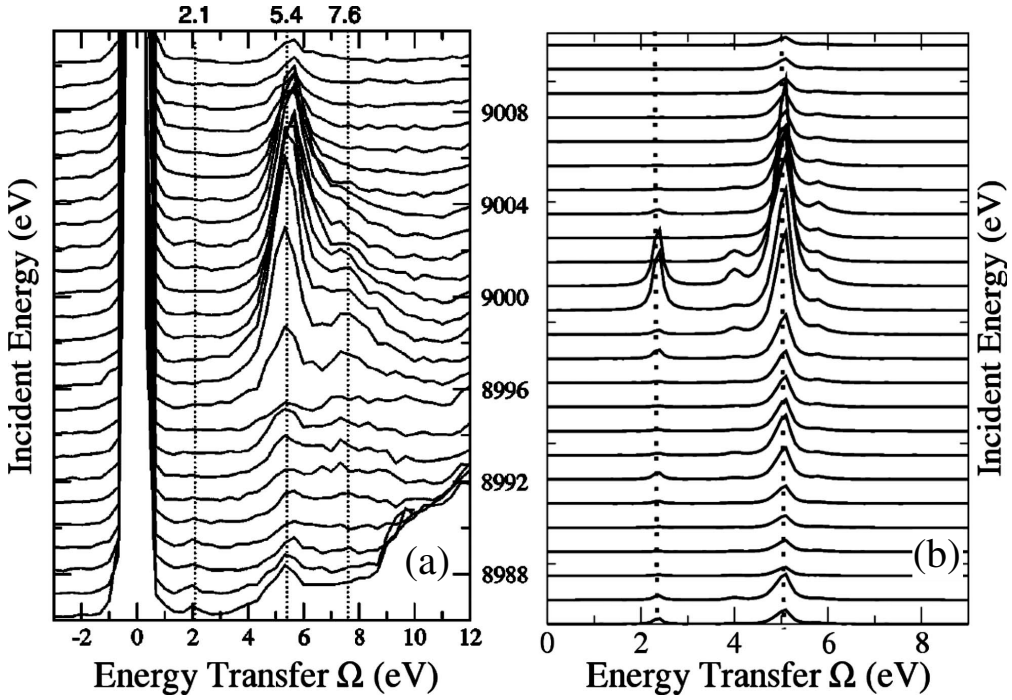

FIG. 4. (a) Experimental data for Li_2CuO_2 by Kim *et al.* in Ref. 8. (b) Calculated RIXS spectrum for parameters corresponding to Li_2CuO_2 convoluted with the $4p$ DOS.

=3.9 eV and Ω=6.2 eV. This energy cost arises from the higher oxygen site energies as well as the reduction in exchange energy gain with the Cu spin.

The $CuGeO_3$ structure in Fig. 6 is different from the one of Li_2CuO_2: the copper chains run now along the c direction and they are tilted from the main-axis planes. We present in Fig. 7(a) the $4p$ projected DOS for $CuGeO_3$. The coordinates system for which the calculation has been done corresponds to the one presented in Fig. 6. As one can see, the result is strongly dependent on polarization: the density of $4p_y$ is peaked around ~8 eV, the $4p_z$ density has its stronger weight around ~18 eV and is much broader.

The corresponding RIXS results are shown for photon polarizations along p_y and p_z in Figs. 7(b) and 7(c), respectively. The overall shape of the spectra does not change much compared to the unconvoluted results (see Fig. 5): one can still identify clearly a low-energy Zhang-Rice peak and a brighter $d^{10}L$ peak at higher energy as well as the poorly screened d^9 excitation peak. The main difference is a shift on the incident photon energy axis, of ~12 eV for p_y and ~21 eV for p_z.

These results are compared to the recent experimental spectrum obtained by Hill *et al.*[25] in Figs. 8 and 9. In this experiment, a CT ($d^{10}L$) peak at $\Omega \approx 6.5$ eV and the ZRS peak as well, closer to the elastic line, at about ~3.8 eV, were identified. These two observed peaks correspond to the two peaks seen in Fig. 5.

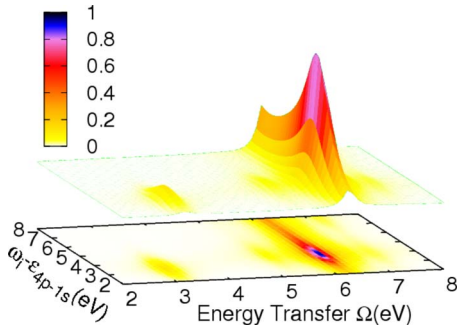

FIG. 5. (Color online) RIXS spectrum as a function of photon energy transfer and incident photon energy for parameters corresponding to $CuGeO_3$, as defined in the text.

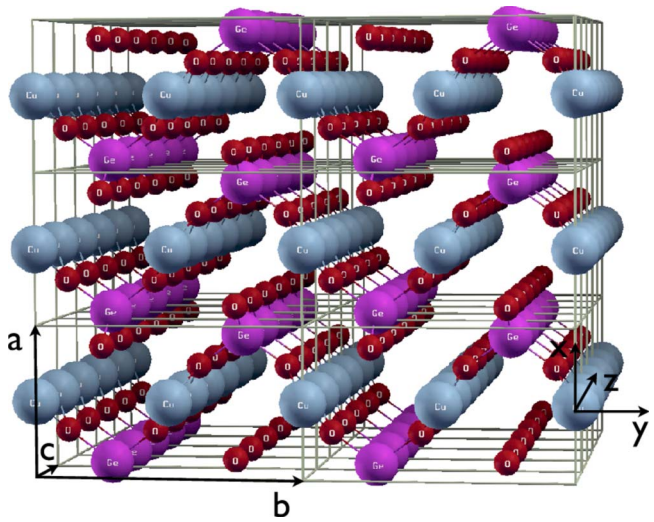

FIG. 6. (Color online) $CuGeO_3$ structure.

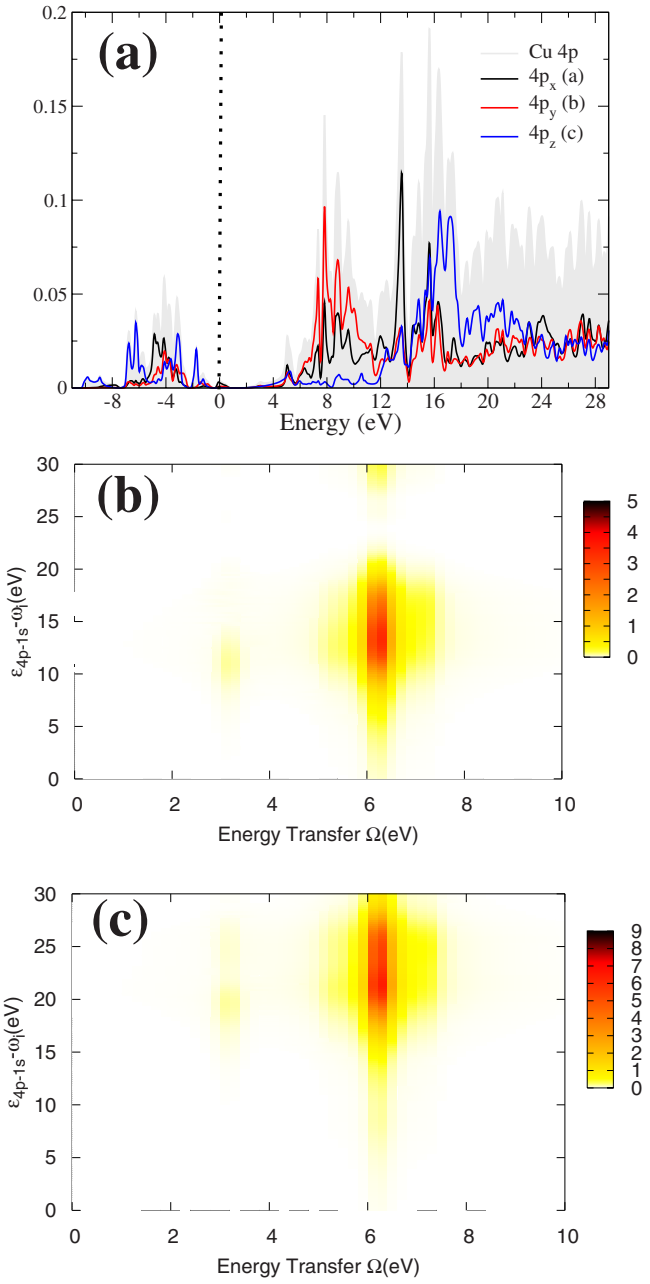

FIG. 7. (Color online) (a) Cu 4*p* partial density of states in $CuGeO_3$ calculated in WIEN2k. (b) RIXS spectrum for parameters corresponding to $CuGeO_3$, convoluted with the p_z-DOS. (c) RIXS spectrum for parameters corresponding to $CuGeO_3$, convoluted with the p_z-DOS.

In Fig. 8 we have used an energy-dependent damping for the Lorentzian representing the delta function of Eq. (1). This energy dependence of the linewidth accounts for the fact that the higher energy states lie in a high density continua. For $\hbar\Omega < 5.5$ eV, a quadratic energy dependence of the damping rate was taken and assumed to saturate at higher Raman shifts. This form was chosen in order to account for the relative intensity and width of the ZR and $d^{10}L$ peaks.

We note that the slight discrepancy between theory and experiment in the position and intensity of the *d*-intersite ZRS may be remedied by fine-tuning the cluster parameters, to more accurately reflect the material properties (such as *J* and the effective ZR hopping *t*), as well as incorporating a more realistic resolution broadening parameter. Another difference between theory and experiment is the relative intensity of the peaks for different polarizations: while the peaks are more intense for a polarization along *b* in the experiment, it is the opposite for the simulation. This issue may be related to the two following points: (i) from a theoretical point of view, the relative intensity of the peaks is sensitively linked to the relative peaks height of the DOS [since in Eq. (1), it appears to be squared], thus a slight variation in the DFT calculation might make a difference. (ii) Due to experimental uncertainties, a direct comparison of the measured absolute intensities for $e\|b$ and $e\|c$ is not possible. However, for a fixed polarization, the measured relative intensities of the ZR and the CT feature can be compared.

Finally, we remark that the crystal structures of $CuGeO_3$ and Li_2CuO_2 are strongly different (see, for instance, Refs. 26 and 27). In both cases, the CuO_2 chains run along a principal axis of the crystal but in $CuGeO_3$ they are not oriented along the same plane, whereas for Li_2CuO_2 they are. This has strong implications concerning the interpretation of the experimental results: for $CuGeO_3$, the polarization-dependent experiments will give RIXS spectra which are a result of convolution with the projected DOS in a rotated basis. The result of such a convolution is given in the right panel of Fig. 9.

IV. CONCLUSIONS

A full exact-diagonalization treatment of multiband Hubbard clusters has been used to calculate the polarization, incident photon energy, and transferred photon energy dependencies of RIXS in one-dimensional, edge-shared insulating cuprates. By building upon previous work,[16] the RIXS spectrum can be constructed using XPS final states as the intermediate states of inelastic x-ray scattering. The intensity and resonance profile, as well as the identity and character of the main RIXS peaks, have been obtained using the eigenstates and eigenenergies of clusters with and without the core hole. These peaks correspond to nonlocally screened *d*-intersite ZRS d^9L, local CT $d^{10}L$, and poorly screened d^9, each having intensities and resonance profile determined by the overlap of these states with the intermediate core-hole states.

The polarization dependent RIXS spectra were obtained by convolving the raw RIXS spectra with the copper 4*p* projected DOS determined by WIEN2K density functional calculations. While the resulting RIXS spectra include the 4*p* states as merely spectators to the rearrangement of copper-oxygen valence charge density, a polarization and material dependent RIXS emerges due to the peak structures and intensities of the 4*p* orbitally projected intermediate states.

Direct comparison (see Figs. 4 and 9) with recent data for two edge-shared cuprates, Li_2CuO_2 and $CuGeO_3$,[8–12] shows both qualitative and, more importantly, quantitative agreements between theory and experiment for the shape, energy, width, and resonance profile of RIXS spectral features. This indicates that the local cluster model can adequately reproduce the data for photon energy losses in the energy range of

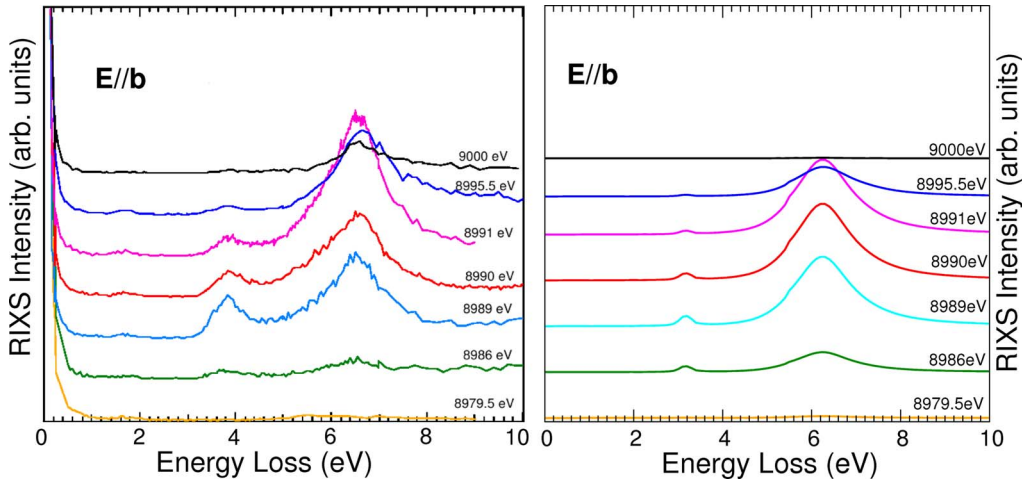

FIG. 8. (Color online) (Left) Experimental RIXS spectrum for $CuGeO_3$. (Right) Theoretical spectrum obtained for the same polarization.

2–7 eV. We again remark that *d-d* excitations are not captured in the model, and further, that spin-flip excitations, which require large clusters to observe bimagnon spin rearrangements at long wavelengths, are also very weak. Better agreement of the calculated spectra with experiment may be obtained by using more refined cluster parameters, multipole couplings, and more accurate representation of resolution broadening.

A polarization dependent RIXS experimental study, for Li_2CuO_2, should find significant differences in the resonant profiles for in-plane polarization and polarization perpendicular to the CuO_2 plane. Figure 3 indicates that peak intensities are brighter and their resonance energies are shifted by ~10 eV for in plane compared to perpendicular polarizations. These predictions as well as others, such as multiple resonant features resulting from 4*p*-projected states, open a way to infer from Cu *K* edge and other indirect RIXS experiments the unoccupied DOS. In this way, RIXS can be seen as a complementary tool to core-level spectroscopies such as XPS and x-ray absorption spectroscopy, providing at the same time diverse and important spectral information on elementary excitations in strongly correlated materials.

In summary, we have explored the Cu *K*-edge spectrum for different edge-shared copper oxide systems, and have

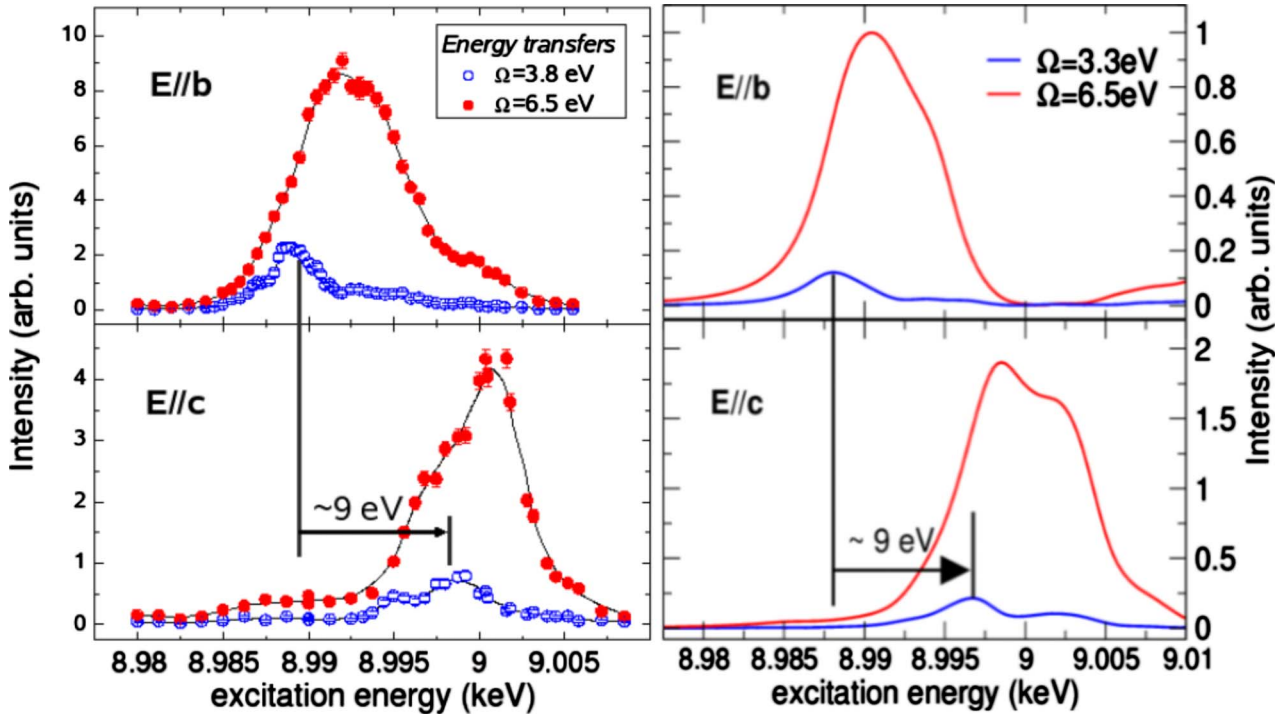

FIG. 9. (Color online) (Left) Experimental RIXS spectrum for $CuGeO_3$ with polarization dependence. (Right) Exact-diagonalization results obtained after convolution with the 4*p* projected DOS of Fig. 7(a) (see Sec. III C).

shown that the energy scales, peak intensities, and resonance profiles can be explained qualitatively within the context of exact diagonalization studies of the multiband Hubbard model. The prospect of mapping out the full momentum and resonance profile dependences would allow for a direct spectral check of the many roles played by local electronic correlations in the multiband Hubbard approach. This remains a topic of future research.

ACKNOWLEDGMENTS

The authors wish to thank J. P. Hill, Y.-J. Kim, Z.-X. Shen, Z. Hussain, M. Z. Hasan, M. Greven, J. Hancock, and M. Gingras for many useful discussions. Use of the Advanced Photon Source was supported by the U. S. Department of Energy, Office of Science, Office of Basic Energy Sciences, under Contract No. DE-AC02-06CH11357. The authors would like to thank T. Gog, D. Casa, and D. Ellis for their support during the experiments at 9ID-B. T.P.D. and G.A.S. would like to acknowledge support of this work in part by NSERC, CFI, ONR Grant N00014-05-1-0127 (T.P.D.), PREA (T.P.D.), the Alexander von Humboldt Foundation (T.P.D.), and CIFAR (G.A.S.). J.G. gratefully acknowledges the financial support by the DFG. T.P.D. wishes to thank the Pacific Institute for Theoretical Physics for their hospitality. F.V. is grateful for the financial support from CIFAR.

*Present address: Stanford Linear Accelerator Center, Stanford University, 2575 Sand Hill Rd., Menlo Park, CA 94025.
†tpd@stanford.edu

[1] A. Damascelli, Z. Hussain, and Z.-X. Shen, Rev. Mod. Phys. **75**, 473 (2003).

[2] J. Graf, G.-H. Gweon, A. Lanzara, Physica C **460**, 194 (2007); J. Graf, G.-H. Gweon, K. McElroy, S. Y. Zhou, C. Jozwiak, E. Rotenberg, A. Bill, T. Sasagawa, H. Eisaki, S. Uchida, H. Takagi, D.-H. Lee, and A. Lanzara, Phys. Rev. Lett. **98**, 067004 (2007); T. Valla, T. E. Kidd, Z.-H. Pan, A. V. Fedorov, W.-G. Yin, G. D. Gu, P. D. Johnson, Phys. Rev. Lett. **98**, 167003 (2007); B. P. Xie, K. Yang, D. W. Shen, J. F. Zhao, H. W. Ou, J. Weil, S. Y. Gu, M. Arita, S. Qiao, H. Namatame, M. Taniguchi, N. Kaneko, H. Eisaki, Z. Q. Yang, D. L. Feng, Phys. Rev. Lett. **98**, 147001 (2007); W. Meevasana, X. J. Zhou, S. Sahrakorpi, W. S. Lee, W. L. Yang, K. Tanaka, N. Mannella, T. Yoshida, D. H. Lu, Y. L. Chen, R. H. He, Hsin Lin, S. Komiya, Y. Ando, F. Zhou, W. X. Ti, J. W. Xiong, Z. X. Zhao, T. Sasagawa, T. Kakeshita, K. Fujita, S. Uchida, H. Eisaki, A. Fujimori, Z. Hussain, R. S. Markiewicz, A. Bansil, N. Nagaosa, J. Zaanen, T. P. Devereaux, and Z.-X. Shen, Phys. Rev. B **75**, 174506 (2007).

[3] T. P. Devereaux and R. Hackl, Rev. Mod. Phys. **79**, 175 (2007).

[4] P. M. Platzmann and E. D. Isaacs, Phys. Rev. B **57**, 11107 (1998); A. Kotani and Shin, Rev. Mod. Phys. **73**, 203 (2001).

[5] F. C. Zhang and T. M. Rice, Phys. Rev. B **37**, 3759 (1988); H. Eskes and G. A. Sawatzky, Phys. Rev. Lett. **61**, 1415 (1988); H. Eskes, L. H. Tjeng, and G. A. Sawatzky, Phys. Rev. B **41**, 288 (1990); H. Eskes and G. A. Sawatzky, *ibid.* **44**, 9656 (1991); P. Horsch, W. H. Stephan, K. v. Szczepanski, and W. von der Linden, Physica C **162**, 783 (1989).

[6] Y. Mizuno, T. Tohyama, S. Maekawa, T. Osafune, N. Motoyama, H. Eisaki, and S. Uchida, Phys. Rev. B **57**, 5326 (1998).

[7] J. B. Goodenough, Phys. Rev. **100**, 564 (1955); J. Kanamori, J. Phys. Chem. Solids **10**, 87 (1959); P. W. Anderson, Solid State Phys. **14**, 99 (1963).

[8] Young-June Kim, J. P. Hill, F. C. Chou, D. Casa, T. Gog, and C. T. Venkataraman, Phys. Rev. B **69**, 155105 (2004).

[9] D. Qian, Y. Li, M. Z. Hasan, D. M. Casa, T. Gog, Y.-D. Chuang, K. Tsutsui, T. Tohyama, S. Maekawa, H. Eisaki, and S. Uchida, J. Phys. Chem. Solids **66**, 2212 (2005).

[10] M. Z. Hasan, Y.-D. Chuang, Y. Li, P. A. Montano, Z. Hussain, G. Dhalenne, A. Revcolevschi, H. Eisaki, N. Motoyama, and S. Uchida, Int. J. Mod. Phys. B **17**, 3519 (2003).

[11] S. Suga, S. Imada, A. Higashiya, A. Shigemoto, S. Kasai, M. Sing, H. Fujiwara, A. Sekiyama, A. Yamasaki, C. Kim, T. Nomura, J. Igarashi, M. Yabashi, and T. Ishikawa, Phys. Rev. B **72**, 081101(R) (2005).

[12] M. v. Zimmermann, J. P. Hill, C.-C. Kao, T. Ruf, G. A. Sawatzky, T. Gog, C. Venkataraman, T. Masuda, I. Tsukada, and K. Uchinokura (unpublished).

[13] L.-C. Duda, J. Downes, C. McGuinness, T. Schmitt, A. Augustsson, K. E. Smith, G. Dhalenne, and A. Revcolevschi, Phys. Rev. B **61**, 4186 (2000).

[14] Kenji Tsutsui, Takami Tohyama, and Sadamichi Maekawa, Phys. Rev. Lett. **91**, 117001 (2003); K. Ishii, K. Tsutsui, Y. Endoh, T. Tohyama, S. Maekawa, M. Hoesch, K. Kuzushita, M. Tsubota, T. Inami, J. Mizuki, Y. Murakami, and K. Yamada, *ibid.* **94**, 207003 (2005).

[15] J. Zaanen, G. A. Sawatzky, and J. W. Allen, Phys. Rev. Lett. **55**, 418 (1985).

[16] M. A. van Veenendaal and G. A. Sawatzky, Phys. Rev. Lett. **70**, 2459 (1993).

[17] M. A. van Veenendaal, H. Eskes, and G. A. Sawatzky, Phys. Rev. B **47**, 11462 (1993); M. van Veenendaal Phys. Rev. B **74**, 085118 (2006); K. Okada and A. Kotani, J. Phys. Soc. Jpn. **75**, 044702 (2006).

[18] Due to the one-dimension geometry of the clusters, especially for the corner-shared case, the d^9L is not truely a ZRS as it has more weight on the central, bridging oxygen. However, the symmetry of this state remains ZR-like, maintaining the ZR signs of the ligands.

[19] Y. Ohta, T. Tohyama, and S. Maekawa, Phys. Rev. B **43**, 2968 (1991); C. Di Castro, L. F. Feiner, and M. Grilli, Phys. Rev. Lett. **66**, 3209 (1991); J. H. Jefferson, H. Eskes, and L. F. Feiner, Phys. Rev. B **45**, 7959 (1992); L. F. Feiner, M. Grilli, and C. Di Castro, *ibid.* **45**, 10647 (1992); R. Raimondi, J. H. Jefferson, and L. F. Feiner, *ibid.* **53**, 8774 (1996).

[20] C. de Graaf and R. Broer, Phys. Rev. B **62**, 702 (2000).

[21] S. Atzkern, M. Knupfer, M. S. Golden, J. Fink, A. Hubsch, C. Waidacher, K. W. Becker, W. vonder Linden, M. Weiden, and C. Geibel, Phys. Rev. B **64**, 075112 (2001).

[22] K. Okada and A. Kotani, Phys. Rev. B **63**, 045103 (2001).

[23] M. W. Haverkort, A. Tanaka, L. H. Tjeng, G. A. Sawatzky, Phys. Rev. Lett. **99**, 257401 (2007).

[24] P. Blaha, K. Schwarz, G. K. H. Madsen, D. Kvasnicka, and J. Luitz, *WIEN2K, An Augmented Plane* Wave+Local *Orbitals Program for Calculating Crystal Properties*, (TU Wien, Austria, 2001).

[25] J. Hill (unpublished).

[26] M. Braden, G. Wilkendorf, J. Lorenzana, M. Ain, G. J. McIntyre, M. Behruzi, G. Heger, G. Dhalenne, and A. Revcolevschi, Phys. Rev. B **54**, 1105 (1996).

[27] F. Sapiña, J. Rodriguez-Carvajal, M. J. Sanchis, R. Ibáñez, A. Beltrán, and D. Beltrán, Solid State Commun. **74**, 779 (1990).